Electrochemical oxidation of ofloxacin using a TiO_2-based SnO_2-Sb/polytetrafluoroethylene resin-PbO_2 electrode: reaction kinetics and mass transfer impact

Ruzhen Xie[a, b], Xiaoyang Meng[b], Peizhe Sun[c], Junfeng Niu[d], Wenju Jiang[a], Lawrence Bottomley[e], Duo Li[f], Yongsheng Chen[c], and John Crittenden[b, *]

[a] College of Architecture and Environment, Sichuan University, Chengdu, Sichuan 610065, China

[b] Brook Byers Institute of Sustainable Systems, School of Civil and Environmental Engineering, Georgia Institute of Technology, Atlanta, GA, 30332, United States

[c] School of Civil and Environmental Engineering, Georgia Institute of Technology, Atlanta, GA, 30332, United States

[d] State Key Laboratory of Water Environment Simulation, School of Environment, Beijing Normal University, Beijing 100875, China

[e] School of Chemistry and Biochemistry, Georgia Institute of Technology, Atlanta, GA 30332, United States

[f] Tech-First, C-305, Building E, Wangjing High-tech Park, LizezhongEr Road, Chaoyang District, Beijing 100102, China

Ruzhen Xie: Email: xieruzhen@scu.edu.cn, Tel: 86-28-8540 3016, Fax: 86-28-8540 5613

Xiaoyang Meng: Email: mxynapoleon@gatech.edu, Tel: 404-894-5676, fax: 404-894-7896

Peizhe Sun: Email: sunpeizhe@gatech.edu, Tel: 404-894-7694, Fax: 404-385-7087

Junfeng Niu: Email: junfengn@bnu.edu.cn, Tel: +86-10-5880 7612, Fax: +86-10-5880 7612

Wenju Jiang: Email: wenjujiang@scu.edu.cn, Tel: 86-28-8540 3016, Fax: 86-28-8540 5613

Lawrence Bottomley: Email: lawrence.bottomley@chemistry.gatech.edu, Tel: 404-894-4041 Fax: 404-894-7452

Duo Li, Email: duo.li@ymail.com, Tel: 010-64398007, Fax: 86-010-84148963

Yongsheng Chen: Email: yongsheng.chen@ce.gatech.edu, Tel: 404-894-3089, Fax: 404-894-2278

Corresponding Author

John Crittenden

Brook Byers Institute of Sustainable Systems, School of Civil and Environmental Engineering, Georgia Institute of Technology, Atlanta, GA, 30332, United States

*e-mail: john.crittenden@ce.gatech.edu. Tel: +1 404 894 5676; fax: +1 404 894 7896.

ABSTRACT

Electrochemical oxidation has been proposed for the destruction of organic contaminants; however, this process is hampered by low oxidation efficiency and high energy cost. Accordingly, we developed a TiO_2-based SnO_2-Sb/polytetrafluroethylene resin (FR)-PbO_2 electrode that was based on TiO_2 nanotubes. We tested the performance of the electrode on an antibiotic, ofloxacin, and identified the major pathway of ofloxacin oxidation. We found growing TiO_2 nanotubes on Ti material increased current efficiency, and the electrical efficiency per order (EE/O, kWh/m^3) for oxidation was decreased by 16.2%. Our electrode requires a large overpotential before electrons flow, which minimizes oxygen evolution, reduces hydrogen peroxide and ozone generation, and favors hydroxyl radicals (HO·) production. We found the electron efficiency (EE) during oxidation was as high as 88.45%. In other words, 88.45% of the electrons that flow out of the electrode cause oxidation. The effects of current density, initial concentration, pH value and electrolyte concentration were investigated. A differential column batch reactor (DCBR) was used to simulate the performance of continuous plug flow reactor and we found that the destruction of ofloxacin followed pseudo-first order model. We also evaluated the impact of mass transfer on electrochemical performance. The effects of fluid velocity and electrode spacing on oxidation rate were evaluated by determining the mass transfer coefficient and the effectiveness factor Ω (between 0-1). Our experiments and calculations indicated that the mass transfer reduced oxidation rate by more than 55% ($\Omega<0.45$) for an electrode spacing of 1 cm at a fluid velocity of 0.033 m/s. Unlike studies carried out using completely mixed batch reactor, the DCBR can simulate the flow conditions in pilot or full scale reactors; consequently, observed pseudo-first order rate constants in the DCBR can be used for preliminary design.

Keywords: Electrochemical oxidation; Ofloxacin; Hydroxyl radicals (HO·); Mass transfer; Effectiveness factor Ω.

1. Introduction

Pharmaceuticals and personal care products (PPCPs) have been recognized as detrimental pollutants because of their potentially hazardous impacts on humans and the environment [1-5]. Many studies have reported the presence of PPCPs in aquatic environments worldwide [1-3]. Antibiotics are among the commonly detected pharmaceuticals in wastewater and other bodies of water subject to pollution from drug manufacturers. These chemicals are considered contaminants because they can lead to antibiotic resistant pathogen communities [4, 5], which can spread their genes to indigenous microbes and increase their antibiotic resistance [6-10]. Therefore, the removal of antibiotics waste water is important. Ofloxacin ($C_{18}H_{20}FN_3O_4$) is one of the most commonly used second-generation topical fluoroquinolones [11]. This antibiotic is a pyridine carboxylic acid derivative of nalidixic acid and has a tricyclic structure with a methyl group at the C-3 position in the oxazine ring. Similar to many other antibiotics, ofloxacin possesses broad-spectrum antibacterial activity that prevents it from being removed effectively by biological treatment plants [12]. Advanced treatment technologies are required to remove/destroy ofloxacin in wastewater.

Advanced oxidation processes (AOPs) are promising technologies for the destruction of organic contaminants in aqueous systems [9, 13, 14]. AOPs produce hydroxyl radicals ($HO^{\cdot}$) at ambient temperature and atmospheric pressure. Electrophilic hydroxyl radicals will react non-selectively with electron-rich organic compounds via hydroxylation and dehydrogenation until the electron-rich organic compounds are completely mineralized to H_2O and CO_2 [15-17]. Consequently, hydroxyl radicals can attack a variety of sites on ofloxacin molecule (e.g., moieties, such as the quinolone moiety) and eventually mineralize them.

Electrochemical oxidation processes have shown an outstanding ability to oxidize and destroy a variety of toxic and refractory organic contaminants [18-21]. These contaminants can be oxidized by the chemisorbed “active oxygen” or “higher oxide” formed on the surface of anodes known as active anodes (e.g., Ti/IrO_2, Ti/RuO_2, and Pt) [22, 23]. The contaminants can also interact directly with the reactive oxygen species (ROSs) physically absorbed on the surface of anodes known as inactive anodes (e.g., Boron-doped diamond (BDD), Ti/SnO_2, and Ti/PbO_2) [18, 22, 24-26]. However, active anodes can more easily form organic films during the degradation and cause anodes fouling. In addition to this aspect, inactive anodes have many other advantages

over active anodes, such as lifetime and oxidation efficiency [26-28]. In recent years, extensive studies have been conducted on inactive anodes with the objective of improving ROSs generation, e.g., by introducing fluoride into PbO_2 layer to have a superhydrophobic-PbO_2 surface will result in greater production of HO· [20, 24]. Some researchers reported enhanced ozone generation during electrolytic process by coating antimony-doped tin dioxide onto a Ti electrode with PbO_2 [25]. Furthermore, using Na_2SO_4 as electrolyte has been shown to produce H_2O_2 generation on Nb/PbO_2 electrode [19].

Quantum theories have been used to explain the creation of ROSs at the anode. During electrolysis, electrons flow from the anode and produce valence band holes (h^+). If the conduction band has a larger energy level than the valence band (such as with a semiconductor), then excitons are produced (i.e., conduction band electrons e^-_{cb} and valence band holes h^+). The band gap determines the power of excitons. Produced valence band holes, in turn, react with water and create ROSs [29, 30]. Anodic oxidation generate ROSs, including oxygen (O_2), hydrogen peroxide (H_2O_2), ozone (O_3) and hydroxyl radicals (HO·), from water [19, 25, 31, 32]. However, dissolved O_2 is a very poor oxidant unless it becomes involved in radical chain reactions that produce other powerful ROSs. H_2O_2 and O_3 can create HO· via a variety of reactions; however, our main objective is to create h^+ with a high enough reduction power that can directly react with water and create HO·. Thus far, BDD anode has been considered as the best inactive anode. It has been shown that the BDD anode has a large band gap (ΔE = 5.45 eV) and it is able to generate a great deal of HO· and lead to a high oxidation efficiency for a variety of different organic contaminant treatments [33]. However, the fabrication of a BDD anode is costly and technically difficult. A titanium-based electrode constructed by coating the SnO_2-Sb material has been shown to exhibit a relatively high oxidation activity as well [34, 35]. Pure SnO_2 is n-type semiconductor with a band gap of 3.5 eV, and its conductivity increases significantly by doping Sb material [36]. Applying a third outer layer of PbO_2 increases the electrochemical stability of the SnO_2-Sb electrode in high voltage; moreover, nano-PbO_2 provides more surface sites for reactions [26, 37]. Ideally, every electron that flows out of the anode should create one hydroxyl radicals if the band gap is large. However, most h^+ and e^-_{cb} recombine before they can undergo chemical reactions on an electrode surface, and the energy supplied is simply wasted. TiO_2 nanotubes (NT) have shown to be an efficient photocatalyst [38].

In addition, reports have shown that the NT exhibits good electron transportation properties and a much lower recombination rate for h^+ and e^-_{cb} [39]. Thus, it would be reasonable to suppose that NT is a good candidate anode material for HO· generation. Besides, introducing NT layer could stabilize the outer layers of the anode [34]. Consequently, we used titanium dioxide NT for the first layer of our electrode.

Although the degradation efficiency can be improved by fabricating novel and active electrodes to enhance electrochemical oxidation, the degradation rate of the observed contaminants is typically lower than that of theoretical calculations. A possible reason for this discrepancy is that batch experiments are usually conducted in a completely mixed system, such as a beaker with stirring. Compared with completely mixed systems, a plug flow reactor (PFR) is used for applications and its mass transfer can be evaluated and improved. We found that mass transfer process significantly reduces the overall reaction rate because oxidation usually occurs on or near the surface of the electrode and reactants have to be transported from the bulk solution to the surface [40]. Compared with the rate of mass transfer, surface reactions are typically much faster. A number of studies have reported that the hydrodynamic design of electrochemical systems influence its oxidation/reduction efficiency, power requirements and total costs due to the mass transfer limitation [41-44]. However, few of these studies have quantified this mass transfer impact by investigating individual hydrodynamic parameters that characterize the reactor, such as electrode spacing and fluid velocity, which are more important among other factors [44, 45]. Without understanding the relationship between mass transfer and oxidation efficiency, the total cost by using different types of electrodes, reactor designs, power requirements, etc., cannot be predicted.

In this study, we fabricate a TiO_2-based SnO_2-Sb/polytetrafluoroethylene resin (FR)-PbO_2 anode that has an overpotential for oxygen evolution higher than the oxygen-forming reduction potential (E^0 = +1.23 V), which means that our anode does not generate O_2. By increasing the applied potential, anodic reactions generate more powerful ROSs, such as H_2O_2 (E^0 = +1.77 V), O_3 (E^0 = +2.07 V) and HO· (E^0 = +2.74 V) [46, 47]. Our approaches to improve the electrochemical performance of anode involve (1) growing TiO_2 NT on Ti foil, (2) implanting a SnO_2-Sb layer on top of the NT layer, and (3) electrodepositing PbO_2 with polytetrafluorethylene resin (FR). The electrochemical oxidation efficiency for ofloxacin degradation is investigated for

various current densities, initial concentrations, pH values and electrolyte concentrations. The reaction kinetics are described using pseudo first-order kinetic model and the energy cost is estimated using the electrical efficiency per order (EE/O or kWh/m^3 per order of contaminant oxidized). The impact of mass transfer is investigated using a differential column batch reactor (DCBR), which simulates the flow condition of a PFR at bench scale. In this study, the laminar flow occurs (Reynolds number, Re<1000), which is a realistic condition for most electrochemical systems [41-44]. The mass transfer coefficient k_f is calculated according to correlations in laminar flow conditions [41]. The effectiveness factor Ω, was used to determine the impact of mass transfer, and it is the ratio of the observed reaction rate to the maximum reaction rate (when there is no mass transfer resistance).

2. Material and methods

All chemicals were analytical reagent grade or higher. Ofloxacin, ethylene glycol (EG), ammonium fluoride (NH_4F), potassium fluoride (KF), lead nitrate ($Pb(NO_3)_2$), tin (IV) chloride, and antimony (III) chloride were purchased from Sigma-Aldrich (St. Louis, MO, USA). The titanium foils (thickness: 0.25 mm, 99.5% purity) were purchased from Alfa Aesar, Haverhill, MA, USA. All solutions were prepared in deionized water (Milli-Q system, 18.2 MΩ-cm).

2.1. Electrode fabrication

The electrode was fabricated in three steps.

Step 1. Grow the TiO_2 NT layer on titanium foil. This step follows the procedure described by Chen et al. [38]. The titanium foil was polished using 2000 grit abrasive paper to obtain a flat surface. The foil was then chemically degreased and etched by immersion in methanol and 6 M nitric acid solution for 5 and 10 min, respectively. The foil was then rinsed using ultrapure water and dried in air at room temperature. The NT array was prepared in a cylindrical electrochemical reactor (250 mL) that was continuously stirred using a magnetic stirrer. The titanium foil (20×50×0.25 mm) was used as anode, and a platinum gauze electrode (40×40×0.5 mm) was used as cathode. The electrodes had a spacing of 20 mm, and the anodization temperature was 60 °C. Ethylene glycol solution containing 0.5 w% NH_4F and 2 v% reagent grade deionized water was used to grow the NT. The anodization was galvanostatically performed using a potentiostat (PowerLab 2/20, AD Instruments) with 10 mA/cm^2 current density for

60 min. The samples were then rinsed in ultrapure water and dried in a nitrogen gas stream. The anatase crystals were formed by calcining the NT in an oxygen atmosphere for 2 h at 500 °C, and then the NT was cooled at a rate of 1 °C/min and hereafter is referred to as the TiO_2-NTs foil.

Step 2. Fabricate Sb-doped SnO_2 intermediate layer over NT. This intermediate layer was created using the sol-gel method according to Lin et al. [27]. The molar ratio of $SnCl_4 \cdot 4H_2O$ to $SbCl_3$ in sol-gel was 9:1. The NT foil was dipped in the sol-gel for 10 min, dried under vacuum at 140 °C and calcined at 500 °C. This process was repeated 15 times before the anode was last annealed for 2 h at 500 °C.

Step 3. Electrodeposition of PbO_2 onto the NT-based SnO_2-Sb electrode. Electrodeposition for the final layer was conducted using an electrolyte containing 0.5 M $Pb(NO_3)_2$, 0.1 M HNO_3, 0.05 M KF and 0.4 mL/L polytetrafluoroethylene resin (FR) [24]. Anodization of the current density was 30 mA/cm^2 for 30 min at 60 °C.

2.2. Electrode characterization

The surface morphology and composition were analyzed using a field emission scanning electron microscope with an energy dispersive spectrometer (FE-SEM, Zeiss Ultra 60 microscope). X-Ray diffraction patterns were measured using a Philips X' pert diffractometer, which was equipped with an Xcelerator module and Cu Kα radiation. X-ray photoelectron spectroscopy (XPS) spectra were measured using a Thermo K-Alpha XPS system and a monochromatic Al Kα source to analyze the electrode surface at a depth of less than 5 nm near the surface. Linear sweep voltammetry (LSV) measurements were conducted at room temperature (25 ± 1 °C) in conventional three-electrode electrochemical cells driven by PARSTAT (Pine Wave Now) at a scan rate of 10 mV/s in 0.5 M H_2SO_4. Our anode served as the working electrode (1 cm × 1 cm), and platinum gauze and Hg/Hg_2Cl_2 (KCl) served as the counter electrode and the reference electrode, respectively.

2.3. Electrochemical oxidation experiments

Our electrochemical reactor was a differential column batch reactor (DCBR). A reservoir contained the test solution, which was pumped through the electrochemical cell and returned to the reservoir. In principle, the DCBR acts as a differential slice of a PFR. We showed that the influent and effluent concentrations of the DCBR were identical. The solution in the reservoir was recirculated using a peristaltic pump, and its

flow rate was adjusted using a stroke rate controller. We sampled the influent, effluent and reservoir simultaneously and their concentrations were similar for different flow rates used in this study (<1%). Therefore, all our samples were collected from the reservoir. The TiO_2-based SnO_2-Sb/FR-PbO_2 electrode (2 cm × 5 cm) was used as the anode and a stainless steel foil (corrosion resistant 316) with the same shape and size served as the cathode. The electrode spacing varied between 0.5 and 3 cm. For each run, an aqueous ofloxacin solution (10-50 mg/L; the volume of solution in the reservoir was 300 mL) containing 0.005-0.5 M Na_2SO_4 electrolyte solution was used. The reservoir was completely mixed (using a magnetic stirrer at 500 revolutions per minute), and the current density was controlled between 5-50 mA/cm^2 using a DC power supply, Extech 382200 and the voltage varied between 3.5 and 8.6 V. The fluid velocity through the electrochemical cell was varied between 0.003 and 0.048 m/s and required a pumping rate between 30 and 576 mL/min, which corresponded to the reservoir detention time of 10.3 min to 0.54 min.

The concentration of ofloxacin was determined using a HPLC-DAD system (Agilent Technologies, series 1200) equipped with a C18 column (Extend, 3.5 µm, 4.63 × 150 mm) operated at a flow rate of 1 mL/min. The mobile phase was composed of 15% HPLC-grade acetonitrile and 85% ultrapure water acidified with 5 mM H_3PO_4. A UV detector set at λ = 287 nm was used to detect the ofloxacin. The sample injection volume was 10 µL.

3. Results and discussion

3.1. Morphology of the TiO_2-based SnO_2-Sb/FR-PbO_2 electrode

Fig. 1 displays the SEM images of the top view of a) TiO_2-nanotubes layer, b) SnO_2-Sb intermediate layer, c) PbO_2 surface layer (without PTFE), and d) polytetrafluoroethylene resin (FR)-PbO_2 surface layer (with PTFE). Fig. 1a shows that the nanotubes are uniformly arranged and have a high density. The top of the nanotubes are open and present circular and oval shapes. The diameters of the nanotubes are between 18 and 22 nm. This thin and uniformed nanotube layer provides tunnels for electrons to reach the inner titanium substrate. Only high-energy electrons that have sufficient power can pass through these tunnels, which theoretically increases the band gap of the anode material. The image in Fig. 1b shows the Sb-doped SnO_2 layer. This

intermediate layer fabricated after dip coating 15 times using sol-gel method and calcination directly over the NT layer. The use of an intermediate layer can reduce the interface resistance between the inner substrate and outer PbO_2 and improve the electrochemical performance [34, 48]. The images in Fig.1c-d are the morphology of deposited PbO_2 without/with polytetrafluoroethylene resin. Fig. 1c shows the surface of coated PbO_2 layer has compact and smooth film that covers the intermediate layer. The addition of PTFE in Fig. 1d introduces hydrophobicity to the electrode, which reduces stress and increases adhesion of PbO_2 to the SnO_2-Sb layer. Besides, during the electrodeposition of PbO_2, the substitution of active oxygen sites by F^- anions inhibit the formation of large crystals. Consequently, the structure of compact F^--PbO_2 provides more surface area, better physical and electrochemical oxidation performance compared with PbO_2 film without PTFE [49]. As Fig. 1d shows, our deposited F^--PbO_2 was uniformly arranged on the anode surface with small crystalline shapes. The thickness of the PbO_2 layer was 71 μm, which was calculated based on the Faraday equation [50].

Fig.1

3.2. Electrode characterization

X-ray diffraction (XRD) was used to estimate the crystal size, and the results are shown in Fig. S1. The XRD result shows that the F^--PbO_2 on the surface has a β-PbO_2 crystallographic structure. The average crystal size of our electrode was calculated as 34.88 nm according to the Scherrer formula, in contrast to the average crystal size for pure PbO_2 is 60.97 nm [51]. Therefore, our electrode has smaller crystals and thus more active sites and surface area.

X-Ray Photoelectron Spectroscopy (XPS) was used to quantify the surface elemental composition and the results are shown in Fig. S2. Fig. S2a shows the XPS spectra of O 1s, reveal a sharp peak centered at 529.08 eV, which correspond to bound (lattice) oxygen. This type of oxygen has been assigned to weakly bound oxygen species [52, 53]. As shown in Fig. S2b, the Pb 4f spectra, exhibits two well defined and symmetric peaks centered at 142.6 eV and 137.5 eV which corresponding to Pb 4f 5/2 and Pb 4f 7/2, respectively. The XPS analysis suggested our anode has an atomic content of 32.72% of Pb on the surface.

Linear sweep voltammetry (LSV) experiments were conducted to evaluate the electrochemical properties of our electrode. Fig. 2 shows the current flow as a function of applied potential on the electrode with/without a TiO_2 NT layer for the purpose of examining the impact of NT regarding ROS generation. The results of both electrodes indicated that a significant current flow did not occur until the voltage increased to 1.5 V. This 1.5 V overpotential for oxygen evolution is higher than the O_2 standard reduction potential (E^0 = +1.23 V at pH = 0), which demonstrates that our electrode does not generate O_2. The LSV results match our bench experiment observations, which did not show oxygen bubble creation during electrolysis. Moreover, this high overpotential for oxygen evolution favors ROS generation. The electrons that flowing out from anode leave valence band holes h^+. These holes are energetic enough to react with water and create more powerful ROS, such as H_2O_2 (E^0 = +1.77 V), O_3 (E^0 = +2.07 V) and (HO·) (E^0 = +2.74 V). With a slight higher overpotential for the anode with nanotubes, it possesses better oxidation ability because it can generate more hydroxyl radicals. In addition, we found that growing nanotubes reduced the total electrical energy usage by up to 16.2% in terms of electrical energy per order of contaminants that was destroyed (EE/O). The observation that introducing TiO_2 nanotubes to increase oxidation current efficiency has been reported in benzoic acid degradation on a TiO_2-NTs/Sb-doped SnO_2 electrode [18].

Fig. 2

3.3. EE/O and oxidation efficiency

Energy efficiency is a critical factor for electrochemical treatment technologies, which usually use a considerable amount of energy cost [54-55]. Evaluating the performance of an electrode based on its electrochemical efficiency and energy efficiency simultaneously is a practical way. The EE/O calculation is used in this study to characterize the energy efficiency of the electrodes and various operational conditions. EE/O is calculated according to the following equation:

$$EE/O = \frac{U \cdot J \cdot A \cdot t}{V \cdot \log(\frac{C_0}{C_t})} \quad (1)$$

where EE/O is the electrical energy required to reduce the concentration of the contaminant by one order of magnitude (kWh/m^3), U is the voltage (V), J is the current density (mA/cm^2), A is the electrode surface area (cm^2), t is the reaction time (h), V is the total volume of the reactor (cm^3), and C_0 and C_t are the concentrations of ofloxacin at the beginning and at time t, respectively (mg/L). We examined the electrochemical performance of the electrode with/without the NT layer and found that both of them can destroy over 99% of 20 mg/L ofloxacin in 90 min in the DCBR under the following operational conditions: anode surface area 10 cm^2, electrode spacing 1 cm, fluid velocity 0.033 m/s, current density 30 mA/cm^2, 0.05 M Na_2SO_4 as electrolyte, pH 6.25, and temperature 25 °C. 92.1% and 90.1% removal efficiency was achieved in the first 60 min for electrode with and without NT layer, respectively. However, we found that the average applied potential on the electrode without NT is 6.8 V, which is obviously higher than the average of 6.2 V for the electrode with NT. By calculating the EE/O for both electrodes, we found that the electrode without TiO_2 NT has an average EE/O of 6.32 kWh/m^3, which is 16.2% higher than the average EE/O of 5.44 kWh/m^3 for the electrode with TiO_2 NT. With regard to energy efficiency, we conducted all of our remaining bench experiments with the electrode containing the TiO_2 NT layer.

To access the degradation efficiency of our electrode, the electron efficiency (EE) η_c was calculated based on Pacheco's method [56]. Electron efficiency represents the efficiency of electrons that are used by the electrode to destroy contaminants during electrolysis. η_c is the ratio of the rate of total organic carbon (TOC) destruction to the rate of chemical oxygen demand (COD) reduction and determines how much oxidation occurs for every electron that leaves the anode.

$$\eta_c = \frac{32}{12} \cdot \left(\frac{n}{4x}\right) \cdot \frac{d(TOC)}{d(COD)} \tag{2}$$

Where TOC is expressed in mg (C)/L, COD is expressed in mg (O_2)/L, and n is the number of electrons transferred from the anode for a complete oxidation reaction. x is the number of carbon atoms in the organic compound.

The stoichiometric equation for ofloxacin is given as:

$$C_{18}H_{20}FN_3O_4 + 41H_2O \rightarrow 18CO_2 + F^- + 3NO_3^- + 102H^+ + 98e^- \tag{3}$$

The ratio $\frac{d(TOC)}{d(COD)}$ for our TiO_2-based SnO_2-Sb/FR-PbO_2 electrode is shown in Fig. S3. The TOC and COD were examined for an operating current density of 30

mA/cm^2 and reactor volume of 310 mL (the DCBR contains a reactor (10 mL) and reservoir (300 mL)), with a flow rate of 400 mL/min (fluid velocity 0.033 m/s), pH of 6.25 and electrolyte concentration of 0.05 M Na_2SO_4. Employing eq. (2) and (3), the EE for the destruction of 20 mg/L of ofloxacin is 88.45% after 2h oxidation. This result demonstrates that during oxidation, 88.45% electrons are effectively used for ofloxacin destruction (i.e., not wasted in O_2 and ROS generation which does not oxidize ofloxacin) and its byproducts are mineralized effectively.

3.4. Oxidation byproduct analysis

The byproducts of the electrochemical oxidation of ofloxacin were investigated and analyzed via liquid chromatography-mass spectrometry (LC-MS), fluoride and TOC mineralization profile was also evaluated. The initial 20 mg/L ofloxacin was completely destroyed, while 53.1% fluorine and 57.36% TOC were mineralized after 120 min. The results shows in Fig. S4. The identification of other organic byproducts are shown in Fig. 3. Five different major byproducts were found and their evolutionary pathways are shown. The m/z value of 362 is ofloxacin. During the initial attack of hydroxyl radicals, a quinolone transformation occurred and yielded P1. A similar reaction occurred in the solar Fenton's treatment of ofloxacin [57]. The pathway for P2 with an m/z of 336 was attributed to a loss of $–C_2H_2$. P3 was formed because of the demethylation of the piperazinyl ring, a mechanism that was also reported for the ofloxacin breakdown caused by a photocatalytic treatment [7]. The inset of Fig. 3 shows a compound with an m/z of 378 is the major byproduct from ofloxacin destruction and represented by P4 in Fig. 3. The formation of P4 is the product of a hydroxyl radicals addition to the ofloxacin piperainyl ring and results in an aldehyde. The results demonstrate that hydroxyl radicals are formed from anodic reactions with our electrode, and hydroxyl radicals are the major oxidizers among other ROS in electrochemical oxidation process using our electrode.

Fig. 3

3.5. Effect of the operational parameters: current density, initial concentration, pH value and electrolyte concentration

Operational conditions influence the performance of electrochemical processes [27]. In the present study, the effects of four major factors, the current density, initial

ofloxacin concentration, pH and electrolyte concentration, were investigated by conducting experiments and fitting the experimental data with pseudo first-order kinetic model. The experiment results for each factor are plotted in Fig. 4a-d. Fitted kinetic rate constants (i.e., pseudo first-order rate constant in this paper) and calculated EE/O results are summarized in Table 1. The impact of temperature on the kinetic rate constants is considered; thus all kinetic experiments were conducted at 25 °C.

The current density is the most important factor in an electrochemical reactor because it determines the energy, energy efficiency with respect to the size of a reactor, resistance of the material, etc. In this work, the impacts of current densities ranging from 5 mA/cm^2 to 50 mA/cm^2 were investigated, and the results are shown in Fig. 4a. As the current density increases, the oxidation rate increases dramatically. The rate constant increases from 0.006 min^{-1} at 5 mA/cm^2 to 0.074 min^{-1} at 50 mA/cm^2. The rate constants vs. current density were plotted and a linear relationship was observed (R^2 = 0.9918). Moreover, by considering the byproducts analysis, which demonstrates that ofloxacin is mainly destroyed through the addition of a hydroxyl radicals to an aromatic ring, it appears that as the current density increases, the production of hydroxyl radicals increases linearly as well. High current densities favor ofloxacin destruction. However, the EE/O results listed in Table 1 show that the electrical energy input almost doubled from 3.78 kWh/m^3 at 5 mA/cm^2 to 6.74 kWh/m^3 at 50 mA/cm^2. A high oxidation rate requires a much higher energy input. From an engineering perspective, the most practical design of a reactor should consider the capital and energy costs simultaneously. As the current density increases, the capital costs should decrease because a smaller treatment device would be used but the energy costs would increase. Consequently, the best design of an electrochemical reactor would minimize the total cost of the operation (capital costs plus operational costs).

Five different initial ofloxacin concentrations were examined for a current density of 30 mA/cm^2. Fig. 4b shows the ofloxacin destruction over time for 10, 20, 30, 40 and 50 mg/L, respectively. The results show that the reaction rate decreases as the initial concentration increases from 10 to 50 mg/L. The EE/O has the same trend as the concentration and increases from 3.66 kWh/m^3 to 15.01 kWh/m^3. Moreover, we found that when the concentration increases from 10 mg/L to 50 mg/L, the rate constants decreases because as ofloxacin is destroyed by hydroxyl radicals, the hydroxyl radicals can further react with the byproducts. The production of hydroxyl radicals is limited by

the input current density. Therefore, a smaller reaction rate is expected as the initial concentration increases.

pH has a considerable impact on the AOP reaction because many radical chain reactions involve the participation of protons [58]. The effect of pH on the electrochemical oxidation of ofloxacin was investigated in a range from pH 4 to pH 11. The results plotted in Fig. 4c show that the ofloxacin destruction rate increases from 0.029 min^{-1} to 0.054 min^{-1} as the pH increases from 4 to 11, and the EE/O also decreases from 6.10 kWh/m^3 to 3.98 kWh/m^3. The reason for this enhancement is because of the decreased hydroxyl radicals' reduction potential, which decreases from 2.74 V at pH 0 to 2.5 V at pH 4. As the applied potential and current density are maintained, more hydroxyl radicals will be generated because the energy barrier for this reaction decreases and more energetic valence band holes on the anode surface become available for the reaction. In addition, the reduction potential further decreases as the pH increases from 4 to 11.

Fig. 4d shows the effect of different electrolyte concentrations on ofloxacin oxidation. Na_2SO_4 was selected as the electrolyte for ofloxacin oxidation to avoid the generation of chlorinated species. When the electrolyte concentration increases from 0.005 M to 0.1 M, the oxidation rate slightly increases. However, when the electrolyte concentration further increases to 0.5 M, the reaction rate decreases significantly. The rate constants were calculated, and a peak was observed at 0.1 M. When the electrolyte concentration increases to 0.5 M, it significantly inhibits oxidation compared with a smaller electrolyte dosage. One possible explanation for this finding is that in an electrochemical system, sulfate ions under high applied potential will produce persulfate, which can significantly scavenge hydroxyl radicals [59, 60]. When the sulfate concentration increases, this inhibition effect becomes significant. The proposed scavenging mechanism reactions are as follows [60]

$$S_2O_8^{2-} + 2e^- \rightarrow 2SO_4^{2-} \qquad E^0 = +2.01\ V \qquad (4)$$

$$S_2O_8^{2-} + HO\cdot \rightarrow HSO_4^- + SO_4^-\cdot + 0.5O_2 \qquad k = 1.2\times10^7\ L\cdot mol^{-1}\cdot s^{-1} \qquad (5)$$

$$SO_4^-\cdot + HO\cdot \rightarrow HSO_5^- \qquad k = 1.0\times10^{10}\ L\cdot mol^{-1}\cdot s^{-1} \qquad (6)$$

Based on the discussion regarding the effect of the current density, initial concentration, pH and electrolyte concentration, this set of operational conditions were identified for further study: current density = 30 mA/cm^2, initial concentration = 20

mg/L, initial pH = 6.25 and electrolyte concentration = 0.05 M. These mild conditions were also used for the investigation of the mass transfer impact.

Fig. 4

Table 1

3.6. Discussion of the mass transfer impact

A number of studies have reported a mass transfer limitation in electrochemical systems [41, 44, 45]. In this study, we quantitatively investigated this impact using a differential column batch reactor (DCBR). A DCBR allows us to conveniently investigate two hydrodynamic factors for the electrochemical reactors: electrode spacing and fluid velocity. These two factors are important because increasing velocities can increase the mass transfer rate and decreasing electrode spacing will increase the surface area per volume of the reactor that is available for mass transfer. Both factors, increasing velocity and decreasing electrode spacing can reduce the impact of mass transfer and increase the reaction rate. Our investigation of these variables is presented in this section.

We used the convective mass transfer coefficient to quantitatively compare the impact of mass transfer. In this study, this coefficient is calculated based on the correlation proposed by Sonin et al. [61] and experimentally confirmed by Grossman et al. [62]. This correlation is essentially equivalent to Leveque's law for heat transfer [41, 61]. Note that this correlation is valid for a reactor geometry length to spacing ratio of less than 126 and Sherwood number (Sh) >>1, which is suitable in the present study.

$$Sh = \frac{k_f \cdot d}{D_l} = 3.3 \cdot (\frac{d}{l} \cdot \mathrm{Re} \cdot Sc)^{\frac{1}{3}} \quad (7)$$

$$\mathrm{Re} = \frac{\rho \cdot u \cdot d}{\mu} \quad (8)$$

$$Sc = \frac{\mu}{\rho \cdot D_l} \quad (9)$$

Where k_f is the mass transfer coefficient (m/s); d is the electrode spacing (hydrodynamic characteristic length of the reactor, m); D_l is the ofloxacin diffusivity, (3.3×10^{-6} cm^2/s), which is calculated using the Hayduk-Laudie correlation (to note that,

ofloxacin is not charged. In other words, the Nernst-Plank equation is not needed in present study; thus diffusion is the only factor cause mass transfer.) [58]; l is the length the fluid travels in the reactor (m); Re is the Reynolds number; Sc is the Schmidt number; u is the fluid velocity (m/s); and ρ and μ are the fluid density (kg/m^3) and fluid dynamic viscosity (kg·m^{-1}·s^{-1}), respectively.

Fig. 5a shows the ofloxacin concentrations as a function of time for different electrode spacings. The pseudo first-order rate constants, EE/O and mass transfer coefficients are plotted in Fig. 5b-c. We examined electrode spacing of 0.5 cm, 1 cm, 2 cm and 3 cm. The fluid velocity was 0.033 m/s, which corresponds to a DCBR detention time of 1.6 s and a reservoir detention time of 45 s. Obviously, the reaction rate increased as the electrode spacing decreased. The pseudo first-order rate constant increased from 0.027 min^{-1} to 0.050 min^{-1} when the electrode spacing decreased from 3 cm to 0.5 cm. We calculated the mass transfer coefficient for different electrode spacing, which explains certain increases in reaction rates. This surface area per reactor volume times the mass transfer coefficient is equal to the first-order destruction rate for a zero concentration of ofloxacin on the surface of the electrode. The mass transfer coefficient increased from 4.43×10^{-6} m/s to 8.05×10^{-6} m/s when the electrode spacing decreased from 3 cm to 0.5 cm. The surface area per volume times the mass transfer coefficient decreased from 8.86×10^{-4} s^{-1} to 2.68×10^{-4} s^{-1} when the electrode spacing increased from 0.5 to 3 cm.

The EE/O also improved with smaller electrode spacing. The EE/O decreased from 21.44 kWh/m^3 to 3.50 kWh/m^3 as the electrode spacing decreased from 3 cm to 0.5 cm. The EE/O decreased significantly because of the decrease of applied electric potential.

Fig. 5

Fig. 6a shows the ofloxacin concentration as a function of time for various fluid velocities. The pseudo first-order rate constant and EE/O are plotted in Fig. 6b-c, respectively. We tested five different fluid velocities: 0.003 m/s, 0.008 m/s, 0.017 m/s, 0.033 m/s and 0.048 m/s. Fig. 6 shows that the reaction rate increases when the fluid velocity increases. The rate constant increases from 0.023 min^{-1} to 0.044 min^{-1} as the fluid velocity increases from 0.003 m/s to 0.048 m/s. The Reynolds number increase as

the fluid velocity increases for a given electrode spacing. Increases in the Reynolds number also increase the Sherwood number and mass transfer coefficient. Our calculations illustrate that the mass transfer coefficient increases dramatically from 2.69×10^{-6} m/s to 7.21×10^{-6} m/s as the velocity increases from 0.003 m/s to 0.048 m/s. Our EE/O calculation excludes the energy use of the stirring reservoir and pumping because our investigation focuses on the energy cost difference that is directly proportional to the mass transfer and these energy inputs are relatively small. The EE/O decreases from 9.50 kWh/m^3 to 4.96 kWh/m^3 as the fluid velocity increases from 0.003 m/s to 0.048 m/s. The results indicate that the increased velocity favors mass transfer processes and enhances the energy efficiency.

Fig. 6

We use the effectiveness factor to determine the impact of mass transfer on the electrochemical oxidation rate. The effectiveness factor is defined by the ratio of the observed reaction rate r_{Obs} to the maximum reaction rate r_{Max} (no mass transfer resistance).

$$\Omega = \frac{r_{Obs}}{r_{Max}} \tag{10}$$

In this study, we used the boundary layer diffusion model to simulate the process of ofloxacin diffusion from the bulk solution to the anode surface [63]. We assume that the ofloxacin concentration C_B does not present a gradient in the bulk solution and that the concentration at the surface of the anode is C_S. The ofloxacin concentration in the diffusion layer C_S is smaller than C_B because of the diffusion restriction, i.e., the mass transfer resistance and reaction that occurs at or near the anode surface. Therefore, we can compare observed reaction rate r_{Obs} and maximum reaction rate r_{Max} as follows:

$$r_{Obs} = k_s \cdot C_S = k \cdot C_B \tag{11}$$

$$r_{Max} = k_s \cdot C_B \tag{12}$$

Where k_s is the surface reaction rate constant (min^{-1}) and k is the observed pseudo first-order rate constant (min^{-1}). Theoretically, the mass transfer rate M_A (mg·L^{-1}·s^{-1}) caused by the surface reaction ($M_A = k_s \cdot C_S$) is equal to the mass transfer rate M_A caused by diffusion from bulk to the surface ($M_A = k_f \cdot a_v \cdot (C_B - C_S)$). k_f is the mass transfer

coefficient (m/s) and a_v is the surface area per volume of the reactor (m^2/m^3). Therefore, the concentration at the electrode surface is C_S is given by this expession:

$$C_S = \frac{k_f \cdot a_v \cdot c_B}{k_f \cdot a_v + k_s} \tag{13}$$

Fig. 1d shows that our anode has a rough surface (larger surface area than a flat plate). Hence, we use a dimensionless surface roughness factor θ to represent the roughness of the anode surface, and the surface area per volume a_v is $\frac{\theta}{d}$ (m^{-1}) in this study. Using Eqs. (11), (12), and (13), the surface reaction rate k_s and roughness factor θ can be determined by fitting the experimental observed pseudo first-order rate constants. Using fitted k_s and observed rate constants, the effectiveness factor Ω for different electrode spacings and fluid velocities can be calculated as follows:

$$k = k_s \cdot \frac{k_f \cdot \theta}{k_f \cdot \theta + k_s \cdot d} \tag{14}$$

$$\Omega = \frac{k}{k_s} \tag{15}$$

Fig. 7 shows the effectiveness factor as a function of the fluid velocity. The mass transfer coefficients for various velocities, k_f, were calculated using the correlation in Eq. (7). These calculations were performed under the conditions of an applied current density of 30 mA/cm^2, initial ofloxacin concentration of 20 mg/L, pH 6.25, electrolyte Na_2SO_4 concentration of 0.05 M and electrode spacing of 1 cm. The surface reaction rate k_s and the roughness factor θ were fitted by minimizing the Objective Function (OF) of the pseudo first-order rate constants in the model and from the data. The parameters k_s and θ in Fig. 7 are 0.0017 s^{-1} (0.1 min^{-1}) and 1.86 in this study, respectively. To confirm the surface roughness factor, we examined the electrode surface using atomic force microscopy (AFM) and estimated the electrode surface area. The surface roughness factor increases as the electrode surface area increases. A larger surface area indicates that more reaction sites (in nm scale) are available. The AFM results are shown in Fig. S5. By assuming that the rough surface obstacles all have the half sphere geometry (smallest geometry compared with pyramid and etc. in same height), the surface area of the electrode is 1.79 times as large as the scanning base area, which is similar to our model fits.

The effectiveness factors reflect the mass transfer resistance, which has a value between 0 and 1. If the value of the effectiveness factor is equal to 1, then the mass transfer resistance is negligible. Fig. 7 shows that the effectiveness factor increases when the fluid velocity increases. The highest examined effectiveness factor (as shown here) was 0.444 at a fluid velocity of 0.048 m/s. These results indicate that the overall electrochemical rate was 55.6% slower than without mass transfer resistance. The effectiveness factors calculated for other operational conditions (e.g., electrode spacing) present similar results as shown in Fig. S6. It was found that the mass transfer reduces the oxidation rate by more than 55% (Ω <0.45) for an electrode spacing of 1 cm at a fluid velocity of 0.033 m/s. Consequently, the mass transfer process has a considerable impact on the overall electrochemical oxidation rate. The rational method presented here that uses the effectiveness factor to evaluate the mass transfer resistance can be applied to other electrochemical systems.

Fig. 7

4. Conclusions

This study reported the fabrication of a TiO_2 NT-based SnO_2-Sb/polytetrafluoroethylene resin (FR)-PbO_2 electrode and its application for the destruction of the antibiotic ofloxacin. To obtain a relatively large band gap and good conductivity, a layer of TiO_2 nanotubes with diameters between 18 and 22 nm were grown on Ti foil and a polytetrafluoroethylene resin material was used to improve the adherence and hydrophobic of the outer PbO_2 layer. The electrode exhibited a high surface area, more oxidation active sites, good electrical conductivity and high oxidation efficiency. Our electrode requires a 1.5 V overpotential before electrons flow, which minimizes oxygen evolution, reduces hydrogen peroxide and ozone generation and favors the production hydroxyl radicals. The results showed that over 99% of 20 mg/L ofloxacin (11.95 mg TOC) can be destroyed after 90 min and the electron efficiency was as high as 88.45%. In other words, 88.45% electrons supplied caused oxidation. A practical operational current density of 30 mA/cm^2 was selected for the batch experiments after simultaneously considering the oxidation rate and energy consumption. The destruction of ofloxacin favors high pH conditions, and its pseudo

first-order rate constants increased by 86% while EE/O decreased by 35% as the pH increases from 4 to 11. This electrochemical oxidation can be run under a relatively low electrolyte condition, e.g., 0.05 M Na_2SO_4. Moreover, the hydrodynamic design of a forced-flow electrochemical system has a significant impact on the mass transfer process. Narrowing the electrode spacing and increasing the fluid velocity will enhance the mass transfer process and increase the overall oxidation rate. The impact of mass transfer was quantified by calculating the mass transfer coefficient and effectiveness factor (This effectiveness factor is the ratio of the observed reaction rate to the surface reaction rate). The experiments and calculations both indicate that the mass transfer reduced the oxidation rate by more than 55% for an electrode spacing of 1 cm at a fluid velocity of 0.033 m/s. Therefore, this study demonstrated the feasibility of using a TiO_2-based SnO_2-Sb/polytetrafluoroethylene resin (FR)-PbO_2 electrode to destroy ofloxacin in the aqueous phase. The derived effectiveness factor can be used in all types of forced-flow electrochemical systems with different electrode types.

ACKNOWLEDGMENT

This research was sponsored by the National Science Foundation Award #0854416. The authors appreciate the Brook Byers Institute for Sustainable Systems, Hightower Chair, and the Georgia Research Alliance at the Georgia Institute of Technology. The authors also acknowledge the advice from Dr. Andaç Armutlulu, Dr. Songyan Du, Mr. Bopeng Zhang and the support of Tech-First. Financial support from the China Scholarship Council for Ruzhen Xie's visiting research in Georgia Institute of Technology is especially acknowledged.

Figure Captions

Fig. 1. SEM of the different layers of the electrode: (a) TiO_2 nanotube layer; (b) SnO_2-Sb intermediate layer; (c) TiO_2-based SbO_2-Sn/FR-PbO_2 electrode surface (without PTFE); and (d) TiO_2-based SnO_2-Sb/FR-PbO_2 electrode surface (with PTFE).

Fig. 2. Linear sweep voltammetry (LSV) of the electrodes with/without the TiO_2 nanotube layer for a 0.5 mol/L H_2SO_4 solution at a scan rate of 10 mV/s; O_2, H_2O_2, O_3 and $HO\cdot$ standard reduction potentials (pH = 0) are 1.23 V, 1.77 V, 2.07 V and 2.74 V, respectively.

Fig. 3. Proposed reaction pathways for the destruction of ofloxacin in electrochemical oxidation. The m/z is the mass/charge ratio. Ofloxacin is 362. Inset graph shows the identification of byproducts.

Fig. 4. Effect of the following operational parameters: (a) current density, (b) initial ofloxacin concentration, (c) pH, (d) Na_2SO_4 concentration. The temperature for all kinetic experiments is 25 °C. The dots are experimental data fitted by pseudo first-order kinetic model lines.

Fig. 5. Effect of electrode spacing: (a) ofloxacin destruction in different electrode spacings, (b) pseudo first-order rate constants, and (c) EE/O. Anode surface area = 10 cm^2, fluid velocity = 0.033 m/s, current density = 30 mA/cm^2, initial ofloxacin concentration = 20 mg/L, voltage = 5-9.2 V, electrolyte concentration = 0.05 M Na_2SO_4 solution, initial pH = 6.25, temperature = 25 °C. The dots are experimental data and fitted by pseudo first-order kinetic model lines.

Fig. 6. Effect of fluid velocity: (a) ofloxacin destruction for different fluid velocities, (b) pseudo first-order rate constants, and (c) EE/O. Anode surface area = 10 cm^2, electrode spacing = 1 cm, electrolyte concentration = 0.05 M Na_2SO_4 solution, current density = 30 mA/cm^2, initial ofloxacin concentration = 20 mg/L, voltage = 6.2-6.3 V, initial pH = 6.25, temperature 25 °C. The dots represetn experimental data fitted by pseudo first-order kinetic model lines.

Fig. 7. Effectiveness factor for different fluid velocities and the best fit model. Anode surface area = 10 cm^2, electrode spacing = 1 cm, electrolyte concentration = 0.05 M Na_2SO_4 solution, current density = 30 mA/cm^2, initial ofloxacin concentration = 20 mg/L, voltage = 6.2-6.3 V, initial pH = 6.25, temperature = 25 °C.

Table Captions

Table 1. Summary of pseudo first-order rate constants, EE/O at different current densities, initial ofloxacin concentrations, pH values and electrolyte Na_2SO_4 concentrations. Operational conditions are current density = 30 mA/cm^2, initial ofloxacin concentration = 20 mg/L, initial pH = 6.25, electrolyte concentration = 0.05 M Na_2SO_4 solution, temperature = 25 °C.

References

[1] T. Lin, S. Yu, W. Chen, Occurrence, removal and risk assessment of pharmaceutical and personal care products (PPCPs) in an advanced drinking water treatment plant (ADWTP) around Taihu Lake in China, Chemosphere 152 (2016) 1-9.

[2] J. Roberts, A. Kumar, J. Du, C. Hepplewhite, D.J. Ellis, A.G. Christy, S.G. Beavis, Pharmaceuticals and personal care products (PPCPs) in Australia's largest inland sewage treatment plant, and its contribution to a major Australian river during high and low flow, Sci. Total Environ. 541 (2016) 1625-1637.

[3] C.I. Kosma, D.A. Lambropoulou, T.A. Albanis, Investigation of PPCPs in wastewater treatment plants in Greece: occurrence, removal and environmental risk assessment, Sci. Total Environ. 466-467 (2014) 421-438.

[4] C. Liu, V. Nanaboina, G. Korshin, Spectroscopic study of the degradation of antibiotics and the generation of representative EfOM oxidation products in ozonated wastewater, Chemosphere (2011).

[5] B. Pan, P. Wang, M. Wu, J. Li, D. Zhang, D. Xiao, Sorption kinetics of ofloxacin in soils and mineral particles, Environ. Pollut. 171 (2012) 185-190.

[6] J. Radjenovic, M. Petrovic, D. Barcelo, Fate and distribution of pharmaceuticals in wastewater and sewage sludge of the conventional activated sludge (CAS) and advanced membrane bioreactor (MBR) treatment, Water Res. 43 (2009) 831-841.

[7] K.H. Wammer, A.R. Korte, R.A. Lundeen, J.E. Sundberg, K. McNeill, W.A. Arnold, Direct photochemistry of three fluoroquinolone antibacterials: norfloxacin, ofloxacin, and enrofloxacin, Water Res. 47 (2013) 439-448.

[8] E.M. Van Wieren, M.D. Seymour, J.W. Peterson, Interaction of the fluoroquinolone antibiotic, ofloxacin, with titanium oxide nanoparticles in water: adsorption and breakdown, Sci. Total Environ. 441 (2012) 1-9.

[9] A. Dirany, I. Sires, N. Oturan, A. Ozcan, M.A. Oturan, Electrochemical treatment of the antibiotic sulfachloropyridazine: kinetics, reaction pathways, and toxicity evolution, Environ. Sci. Technol. 46 (2012) 4074-4082.

[10] M. Chen, W. Chu, Photocatalytic degradation and decomposition mechanism of fluoroquinolones norfloxacin over bismuth tungstate: Experiment and mathematic model, Appl. Catal. B:Environ. 168-169 (2015) 175-182.

[11] T.S. Chen, K.L. Huang, J.L. Chen, An electrochemical approach to simultaneous determination of acetaminophen and ofloxacin, Bull. Environ. Contam. Toxicol. 89 (2012) 1284-1288.

[12] M. Imamura, S. Shibamura, I. Hayakawa, Y. Osada, Inhibition of DNA gyrase by optically active ofloxacin, Antimicrob. Agents Chemother. 31 (1987) 325-327.

[13] C. Carlesi Jara, D. Fino, V. Specchia, G. Saracco, P. Spinelli, Electrochemical removal of antibiotics from wastewaters, Appl. Catal. B:Environ. 70 (2007) 479-487.

[14] C. Borras, C. Berzoy, J. Mostany, J.C. Herrera, B.R. Scharifker, A comparison of the electrooxidation kinetics of p-methoxyphenol and p-nitrophenol on Sb-doped SnO_2 surfaces: Concentration and temperature effects, Appl. Catal. B:Environ. 72 (2007) 98-104.

[15] X. Guo, D. Minakata, J. Crittenden, Computer-based first-principles kinetic Monte Carlo simulation of polyethylene glycol degradation in aqueous phase UV/H_2O_2 advanced oxidation process, Environ. Sci. Technol. 48 (2014) 10813-10820.

[16] X. Guo, D. Minakata, J. Crittenden, On-the-Fly Kinetic Monte Carlo Simulation of Aqueous Phase Advanced Oxidation Processes, Environ. Sci. Technol. 49 (2015) 9230-9236.
[17] X. Guo, D. Minakata, J. Niu, J. Crittenden, Computer-based first-principles kinetic modeling of degradation pathways and byproduct fates in aqueous-phase advanced oxidation processes, Environ. Sci. Technol. 48 (2014) 5718-5725.
[18] G. Zhao, X. Cui, M. Liu, P. Li, Y. Zhang, T. Cao, H. Li, Y. Lei, L. Liu, D. Li, Electrochemical Degradation of Refractory Pollutant Using a Novel Microstructured TiO_2 Nanotubes/Sb-Doped SnO_2 Electrode, Environ. Sci. Technol., 43 (2009) 1480-1486.
[19] H. Yang, J. Liang, L. Zhang, Z. Liang, Electrochemical Oxidation Degradation of Methyl Orange Wastewater by Nb/PbO2 Electrode, Int. J. Electrochem. Ci., 11 (2016) 1121-1134.
[20] Y. Lei, G. Zhao, Y. Zhang, M. Liu, L. Liu, B. Lv, J. Gao, Highly efficient and mild electrochemical incineration: mechanism and kinetic process of refractory aromatic hydrocarbon pollutants on superhydrophobic PbO(2) anode, Environ. Sci. Technol., 44 (2010) 7921-7927.
[21] E. Brillas, I. Sires, M.A. Oturan, Electro-Fenton process and related electrochemical technologies based on Fenton's reaction chemistry, Chem. Rev. 109 (2009) 6570-6631.
[22] G. Zhao, S. Shen, M. Li, M. Wu, T. Cao, D. Li, The mechanism and kinetics of ultrasound-enhanced electrochemical oxidation of phenol on boron-doped diamond and Pt electrodes, Chemosphere 73 (2008) 1407-1413.
[23] I.D. Santos, M. Dezotti, A.J.B. Dutra, Electrochemical treatment of effluents from petroleum industry using a Ti/RuO_2 anode, Chem. Eng. J. 226 (2013) 293-299.
[24] G. Zhao, Y. Zhang, Y. Lei, B. Lv, J. Gao, Y. Zhang, D. Li, Fabrication and electrochemical treatment application of a novel lead dioxide anode with superhydrophobic surfaces, high oxygen evolution potential, and oxidation capability, Environ. Sci. Technol., 44 (2010) 1754-1759
[25] S.A Cheng, K.Y. Chan, Electrolytic Generation of Ozone on and Antimony-Doped Tin Dioxide Coated Electrode, Electrochem. Solid. ST., 7 (2004) D4-D6.
[26] A. Mukimin, K. Wijaya, A. Kuncaka, Oxidation of remazolbrilliant bluer(RB.19) with in situ electro-generated active chlorine using Ti/PbO_2 electrode, Sep. Purif. Technol. 95 (2012) 1-9.
[27] H. Lin, J. Niu, J. Xu, Y. Li, Y. Pan, Electrochemical mineralization of sulfamethoxazole by Ti/SnO_2-Sb/Ce-PbO_2 anode: Kinetics, reaction pathways, and energy cost evolution, Electrochim. Acta 97 (2013) 167-174.
[28] G. Zhao, J. Gao, S. Shen, M. Liu, D. Li, M. Wu, Y. Lei, Ultrasound enhanced electrochemical oxidation of phenol and phthalic acid on boron-doped diamond electrode, J. Hazard. Mater. 172 (2009) 1076-1081.
[29] D. Lawless, N. Serpone, D. Meisel, Role of hydroxyl radicals and trapped holes in photocatalysis. A pulse radiolysis study, J. Phys. Chem. 95 (1991) 5166-5170.
[30] Q. Xiao, Z. Si, J. Zhang, C. Xiao, X. Tan, Photoinduced hydroxyl radical and photocatalytic activity of samarium-doped TiO(2) nanocrystalline, J. Hazard. Mater. 150 (2008) 62-67.
[31] G.V. Buxton, C.L. Greenstock, W.P. Helman, A.B. Ross, W. Tsang, Critical Review of rate constants for reactions of hydrated electronsChemical Kinetic Data Base for Combustion Chemistry. Part 3: Propane, J. Phys. Chem. Ref. Data 17 (1988) 513.

[32] J.M. Peralta-Hernández, C. de la Rosa-Juárez, V. Buzo-Muñoz, J. Paramo-Vargas, P. Cañizares-Cañizares, M.A. Rodrigo-Rodrigo, Synergism between anodic oxidation with diamond anodes and heterogeneous catalytic photolysis for the treatment of pharmaceutical pollutants, Sustain. Environ. Res. (2016).
[33] F. Beck, W. Kaiser, H. Krohn, Boron doped diamond (BDD)-layers on titanium substrates as electrodes in applied electrochemistry, Electrochim. Acta 45 (2000) 4691-4695.
[34] X. Cui, G. Zhao, Y. Lei, H. Li, P. Li, M. Liu, Novel vertically aligned TiO2 nanotubes embedded with Sb-doped SnO2 electrode with high oxygen evolution potential and long service time, Materials Chemistry and Physics, 113 (2009) 314-321.
[35] S. Song, J. Fan, Z. He, L. Zhan, Z. Liu, J. Chen, X. Xu, Electrochemical degradation of azo dye C.I. Reactive Red 195 by anodic oxidation on Ti/SnO_2–Sb/PbO_2 electrodes, Electrochim. Acta 55 (2010) 3606-3613.
[36] M.M. Halmann, Photodegradation of Water Pollutants, CRC Press, Baca Raton, New York, 1996, pp. 285.
[37] C. Zhong, K. Wei, W. Han, L. Wang, X. Sun, J. Li, Electrochemical degradation of tricyclazole in aqueous solution using Ti/SnO_2–Sb/PbO_2 anode, J. Electroanal. Chem. 705 (2013) 68-74.
[38] Y. Chen, J.C. Crittenden, S. Hackney, L. Sutter, D.W. Hand, Preparation of a Novel TiO_2-Based p−n Junction Nanotube Photocatalyst, Environ. Sci. Technol. 39 (2005) 1201-1208.
[39] S. Herna´ndez, D. Hidalgo, A. Sacco, A. Chiodoni, A. Lamberti, V. Cauda, E. Tressoa, G. Saracco, Comparison of photocatalytic and transport properties of TiO_2 and ZnO nanostructures for solar-driven water splitting Phys. Chem. Chem. Phys. 17 (2015) 7775-7786.
[40] C.G. Zoski, Handbook of Electrochemistry, Elsevier, Amsterdam,Boston, 2007, pp. 11-13.
[41] A.A. Sonin, M.S. Isaacson, Optimization of Flow Design in Forced Flow Electrochemical Systems, with Special Application to Electrodialysis, Ind. Eng. Chem. Process Des. Dev. 13 (1974) 241-248.
[42] W. Djoudi, F. Aissani-Benissad, P. Ozil, Flow modeling in electrochemical tubular reactor containing volumetric electrode: Application to copper cementation reaction, Chem. Eng. Res. Des. 90 (2012) 1582-1589.
[43] U.M. López-García, P.E. Hidalgo, J.C. Olvera, F. Castañeda, H. Ruiz, G. Orozco, The hydrodynamic behavior of a parallel-plate electrochemical reactor, Fuel 110 (2013) 162-170.
[44] J.Y. Choi, Y.J. Lee, J. Shin, J.W. Yang, Anodic oxidation of 1,4-dioxane on boron-doped diamond electrodes for wastewater treatment, J. Hazard. Mater. 179 (2010) 762-768.
[45] L. Ciríaco, C. Anjo, J. Correia, M.J. Pacheco, A. Lopes, Electrochemical degradation of Ibuprofen on Ti/Pt/PbO_2 and Si/BDD electrodes, Electrochim. Acta 54 (2009) 1464-1472.
[46] A.J. Bard, R. Parsons, J. Jordan, Standard potentials in aqueous solution, CRC press, New York, 1985.
[47] W.H. Koppenol, J.F. Liebman, The oxidizing nature of the hydroxyl radical. A comparison with the ferryl ion (FeO^{2+}), J. Phys. Chem. 88 (1984) 99-101.
[48] P. Li, G. Zhao, X. Cui, Y. Zhang, Y. Tang, Constructing Stake Structured TiO_2-NTs/Sb-Doped SnO2 Electrode Simultaneously with High Electrocatalytic and

Photocatalytic Performance for Complete Mineralization of Refractory Aromatic Acid, J. Phys. Chem.C, 113 (2009) 2375-2383.
[49] M. Panizza, G. Cerisola, Direct and mediated anodic oxidation of organic pollutants, Chem. Rev. 109 (2009) 6541-6569.
[50] T. Raju, C.A. Basha, Electrochemical cell design and development for mediated electrochemical oxidation-Ce(III)/Ce(IV)system, Chem. Eng. J. 114 (2005) 55-65.
[51] J. Cao, H. Zhao, F. Cao, J. Zhang, C. Cao, Electrocatalytic degradation of 4-chlorophenol on F-doped PbO_2 anodes, Electrochim. Acta 54 (2009) 2595-2602.
[52] Y. Liu, H. Liu, J. Ma, J. Li, Investigation on electrochemical properties of cerium doped lead dioxide anode and application for elimination of nitrophenol, Electrochim. Acta, 56 (2011) 1352-1360.
[53] S. Chai, G. Zhao, Y. Wang, Y.-n. Zhang, Y. Wang, Y. Jin, X. Huang, Fabrication and enhanced electrocatalytic activity of 3D highly ordered macroporous PbO_2 electrode for recalcitrant pollutant incineration, Appl. Catal. B:Environ., 147 (2014) 275-286.
[54] J. Radjenovic, D.L. Sedlak, Challenges and Opportunities for Electrochemical Processes as Next-Generation Technologies for the Treatment of Contaminated Water, Environ. Sci. Technol. 49 (2015) 11292-11302.
[55] X. Zhu, J. Ni, J. Wei, X. Xing, H. Li, Y. Jiang, Scale-up of BDD anode system for electrochemical oxidation of phenol simulated wastewater in continuous mode, J. Hazard. Mater 184 (2010) 493-498.
[56] M.J. Pacheco, A. Morão, A. Lopes, L. Ciríaco, I. Gonçalves, Degradation of phenols using boron-doped diamond electrodes: A method for quantifying the extent of combustion, Electrochim. Acta 53 (2007) 629-636.
[57] I. Michael, E. Hapeshi, J. Acena, S. Perez, M. Petrovic, A. Zapata, D. Barcelo, S. Malato, D. Fatta-Kassinos, Light-induced catalytic transformation of ofloxacin by solar Fenton in various water matrices at a pilot plant: mineralization and characterization of major intermediate products, Sci. Total Environ. 461-462 (2013) 39-48.
[58] John C. Crittenden, R. Rhodes Trussell, David W. Hand, Kerry J. Howe, G. Tchobanoglous, MWH's Water Treatment: Principles and Design, 3rd Ed., John Wiley &Sons, Inc., Hoboken, New Jersey, 2012.
[59] I. Peternel, H. Kusic, V. Marin, N. Koprivanac, UV-assisted persulfate oxidation: the influence of cation type in the persulfate salt on the degradation kinetics of an azo dye pollutant, React. Kinet. Mech. Cat. 108 (2012) 17-39.
[60] T.N. Das, Reactivity and Role of $SO_5^{\bullet-}$Radical in Aqueous Medium Chain Oxidation of Sulfite to Sulfate and Atmospheric Sulfuric Acid Generation, J. Phys. Chem. A 105 (2001) 9142-9155.
[61] R.F.P. Ain A. Sonin, A hydrodynamic theory of desalination by electrodialysis, Desalination 5 (1968) 293-329.
[62] A.A.S. Gershon Grossman, Experimental study of the effects of hydrodynamics and membrane fouling in electrodialysis, Desalination 10 (1972) 157-180.
[63] H.S. Fogler, Elements of chemical reaction engineering, 2nd Ed., Prentice-HallInternational,Inc.,NewJersey, 1992.

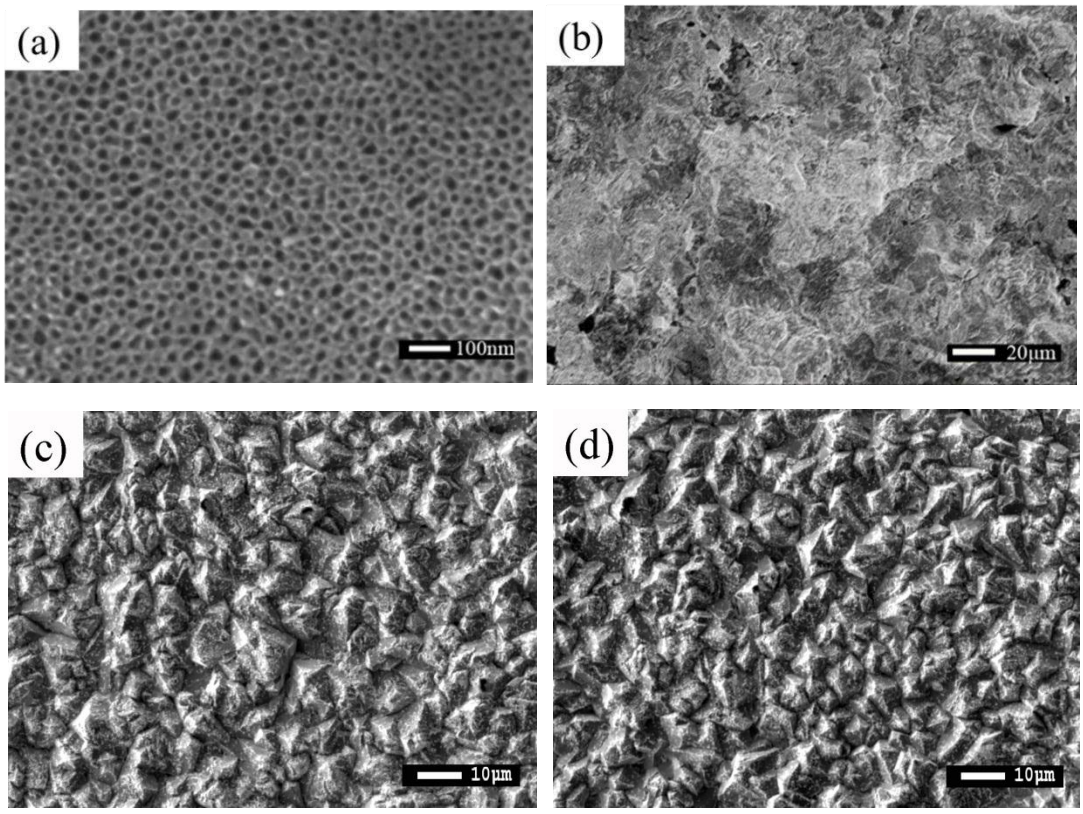

Fig. 1. SEM of the different layers of the electrode: (a) TiO_2 nanotube layer; (b) SnO_2-Sb intermediate layer; (c) TiO_2-based SnO_2-Sb/PbO_2 electrode surface (without PTFE); and (d) TiO_2-based SnO_2-Sb/FR-PbO_2 electrode surface (with PTFE).

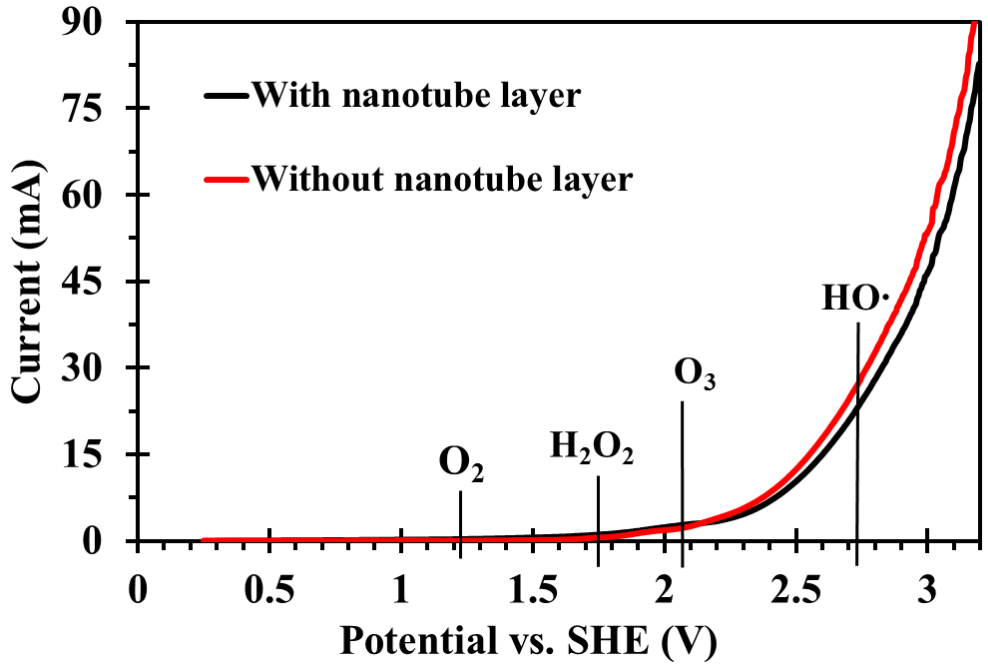

Fig. 2. Linear sweep voltammetry (LSV) of the electrodes with/without the TiO_2 nanotube layer for a 0.5 mol/L H_2SO_4 solution at a scan rate of 10 mV/s; O_2, H_2O_2, O_3 and HO· standard reduction potentials (pH = 0) are 1.23 V, 1.77 V, 2.07 V and 2.74 V, respectively.

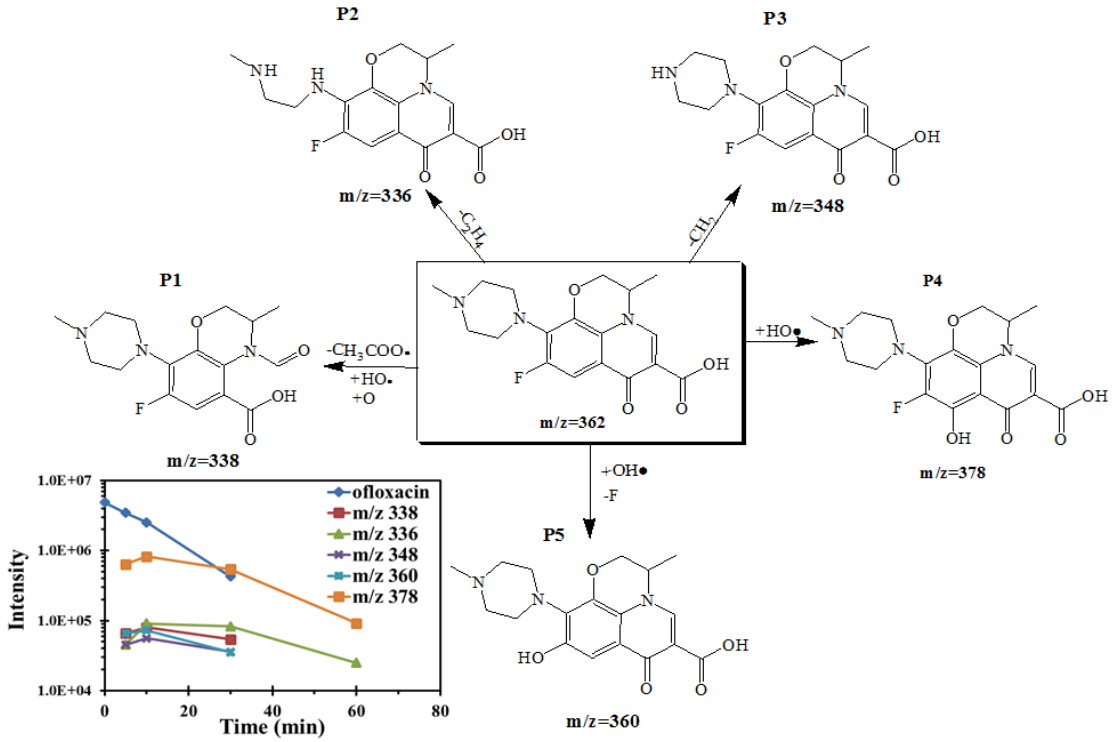

Fig. 3. Proposed reaction pathways for the destruction of ofloxacin in electrochemical oxidation. The m/z is the mass/charge ratio. Ofloxacin is 362. Inset graph shows the identification of byproducts.

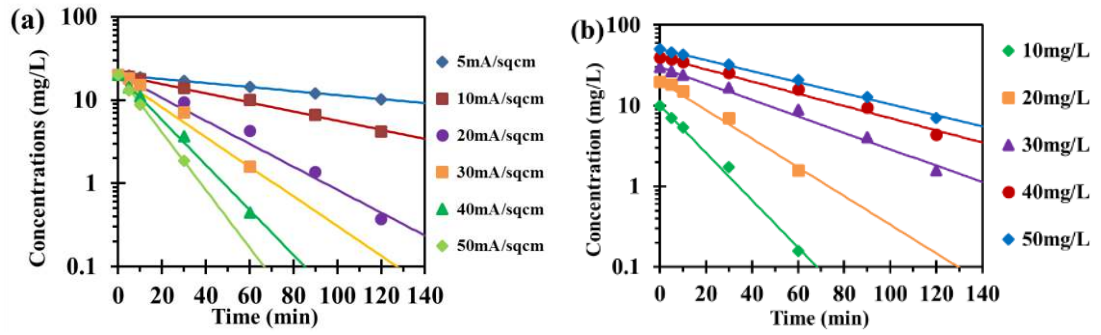

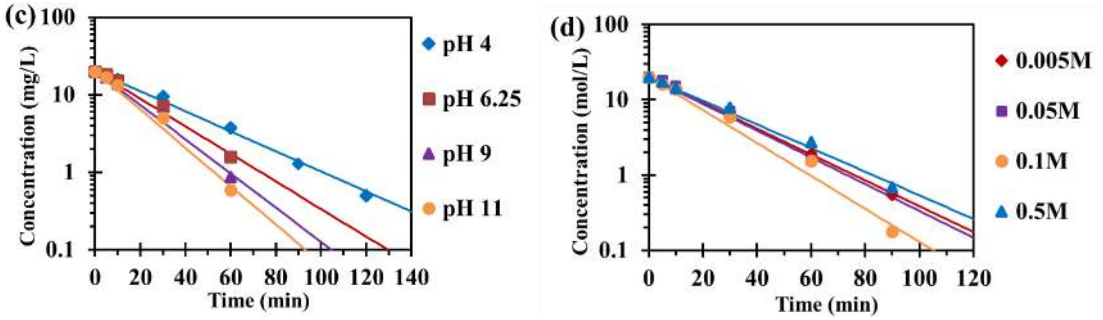

Fig. 4. Effect of the following operational parameters: (a) current density, (b) initial ofloxacin concentration, (c) pH, (d) electrolyte Na_2SO_4 concentration. The temperature for all kinetic experiments is 25 °C. The dots are experimental data fitted by pseudo first-order kinetic model lines.

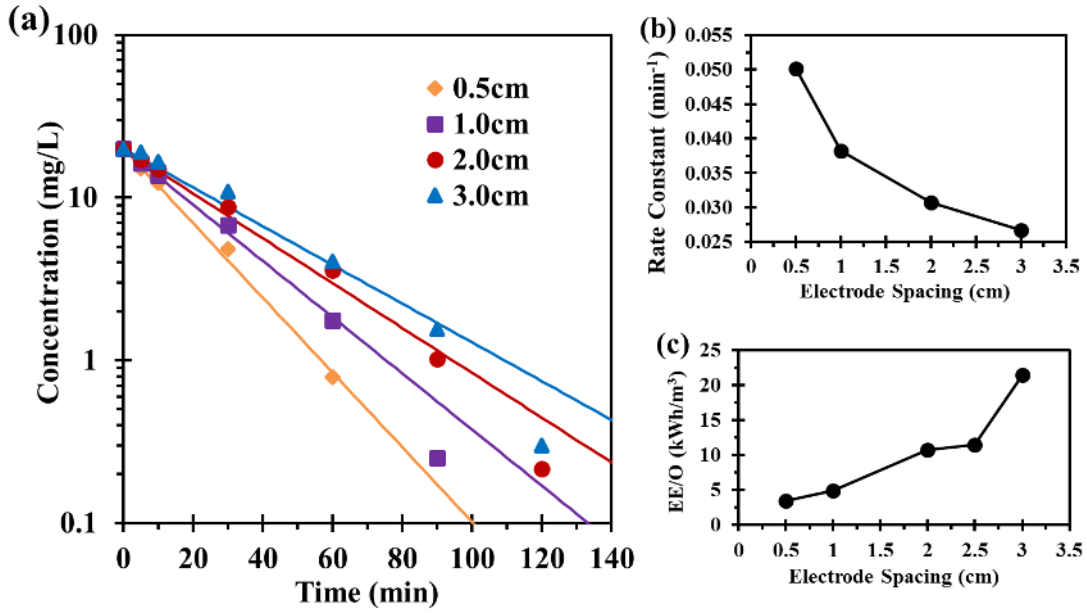

Fig. 5. Effect of electrode spacing: (a) ofloxacin destruction in different electrode spacing, (b) pseudo first-order rate constants, and (c) EE/O. Anode surface area = 10 cm^2, fluid velocity = 0.033 m/s, current density = 30 mA/cm^2, initial ofloxacin concentration = 20 mg/L, voltage = 5-9.2 V, electrolyte concentration = 0.05 M Na_2SO_4 solution, initial pH = 6.25, temperature = 25 °C. The dots are experimental data and fitted by a pseudo first-order kinetic model lines.

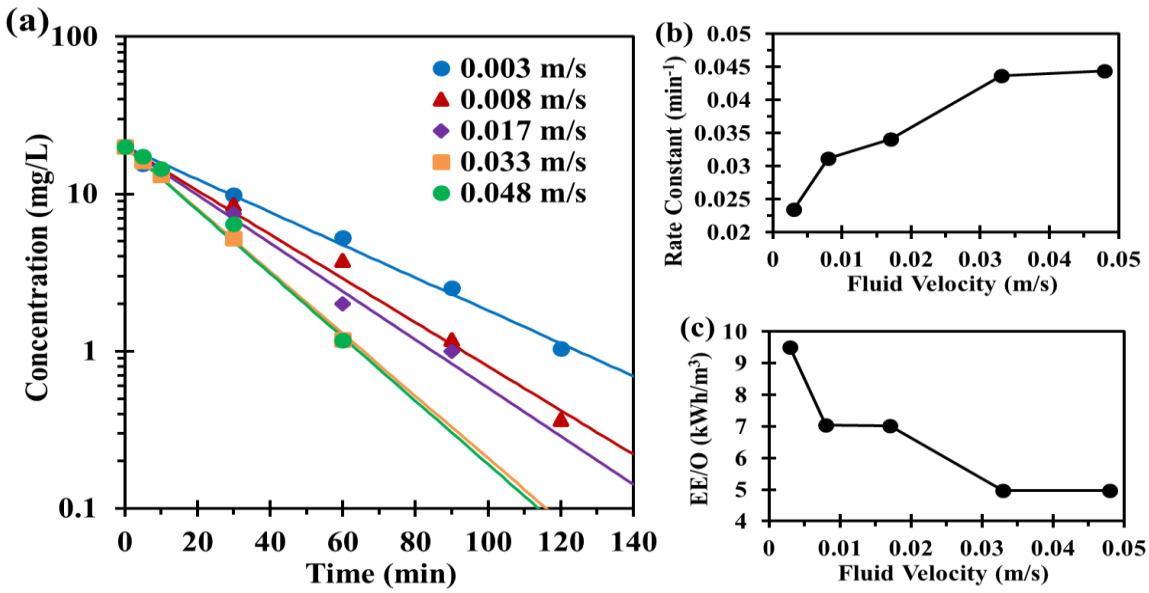

Fig. 6. Effect of fluid velocity: (a) ofloxacin destruction for different fluid velocities, (b) pseudo first-order rate constants, and (c) EE/O. Anode surface area = 10 cm^2, electrode spacing = 1 cm, electrolyte concentration = 0.05 M Na_2SO_4 solution, current density = 30 mA/cm^2, initial ofloxacin concentration = 20 mg/L, voltage = 6.2-6.3 V, initial pH = 6.25, temperature 25 °C. The dots represent experimental data fitted by a pseudo first-order kinetic model lines.

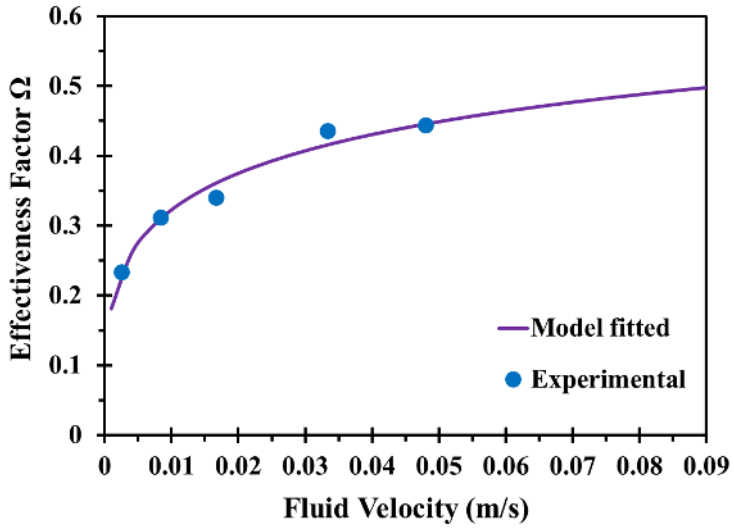

Fig. 7. Effectiveness factor for different fluid velocities and the best fit model. Anode surface area = 10 cm^2, electrode spacing = 1 cm, electrolyte concentration = 0.05 M Na_2SO_4 solution, current density = 30 mA/cm^2, initial ofloxacin concentration = 20 mg/L, voltage = 6.2-6.3 V, initial pH = 6.25, temperature = 25 °C.

	Current density (mA/cm^2)						pH			
	5	10	20	30	40	50	4	6.25	9	11
Pseudo first-order rate constants (min^{-1})	0.006	0.013	0.032	0.039	0.059	0.074	0.029	0.039	0.048	0.054
Electric efficiency per order (EE/O) (kWh/m^3)	3.78	3.91	4.25	5.26	5.64	6.74	6.10	5.44	4.48	3.98
	Initial concentration (mg/L)						Na_2SO_4 concentration (M)			
	10	20	30	40	50		0.005	0.05	0.1	0.5
Pseudo first-order rate constants (min^{-1})	0.063	0.039	0.023	0.017	0.016		0.038	0.039	0.048	0.035
Electric efficiency per order (EE/O) (kWh/m^3)	3.66	5.44	9.69	12.88	15.01		23.41	5.44	5.26	2.98

Table 1. Summary of pseudo first-order rate constants, EE/O at different current densities, initial ofloxacin concentrations, pH values and electrolyte Na_2SO_4 concentrations. Operational controlled conditions are current density = 30 mA/cm^2, initial ofloxacin concentration = 20 mg/L, initial pH = 6.25, electrolyte concentration = 0.05 M Na_2SO_4 solution, temperature = 25 °C.

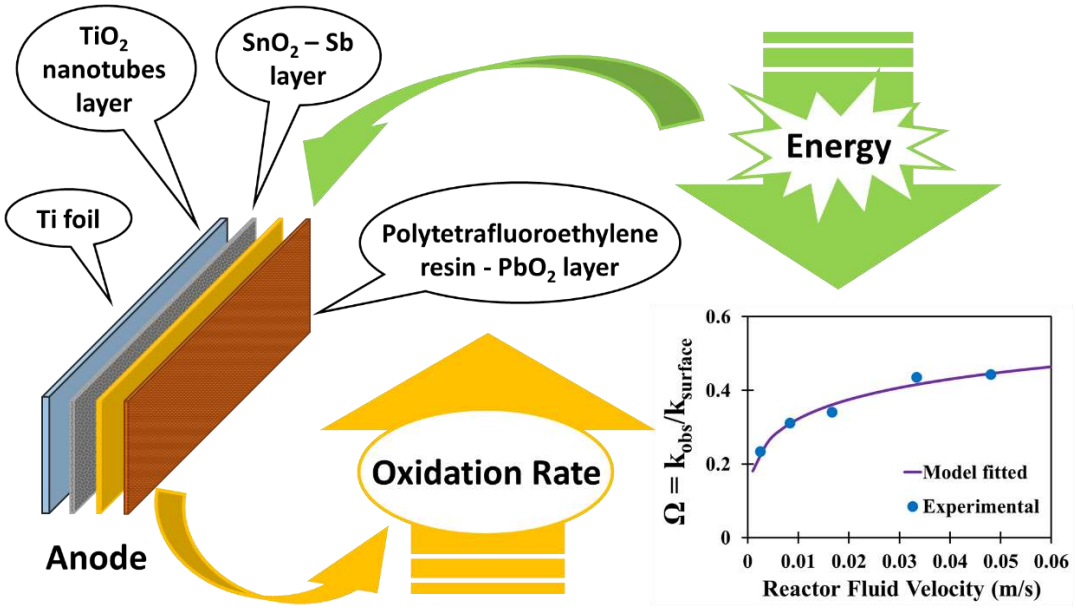
TiO2 nanotubes layer
SnO2 – Sb layer
Ti foil
Polytetrafluoroethylene resin - PbO2 layer
Energy
Oxidation Rate
Anode
Ω = kobs/ksurface
0.6
0.4
0.2
0
0 0.01 0.02 0.03 0.04 0.05 0.06
Model fitted
Experimental
Reactor Fluid Velocity (m/s)